

Emergent second law for non-equilibrium steady states

Nahuel Freitas¹ and Massimiliano Esposito¹

¹*Complex Systems and Statistical Mechanics, Department of Physics and Materials Science,
University of Luxembourg, L-1511 Luxembourg, Luxembourg*

(Dated: June 20, 2022)

The Gibbs distribution universally characterizes states of thermal equilibrium. In order to extend the Gibbs distribution to non-equilibrium steady states, one must relate the self-information $\mathcal{I}(x) = -\log(P_{\text{ss}}(x))$ of microstate x to measurable physical quantities. This is a central problem in non-equilibrium statistical physics. By considering open systems described by stochastic dynamics which become deterministic in the macroscopic limit, we show that changes $\Delta\mathcal{I} = \mathcal{I}(x_t) - \mathcal{I}(x_0)$ in steady state self-information along deterministic trajectories can be bounded by the macroscopic entropy production Σ . This bound takes the form of an emergent second law $\Sigma + k_b\Delta\mathcal{I} \geq 0$, which contains the usual second law $\Sigma \geq 0$ as a corollary, and is saturated in the linear regime close to equilibrium. We thus obtain a tighter version of the second law of thermodynamics that provides a link between the deterministic relaxation of a system and the non-equilibrium fluctuations at steady state. In addition to its fundamental value, our result leads to novel methods for computing non-equilibrium distributions, providing a deterministic alternative to Gillespie simulations or spectral methods.

I. INTRODUCTION

When a system is at equilibrium with its environment (i.e., when no energy currents are exchanged) the probability of a given microstate \mathbf{x} is given by the Gibbs distribution [1–3]

$$P_{\text{eq}}(\mathbf{x}) = e^{-\beta\Phi(\mathbf{x})}/Z, \quad (1)$$

where $\beta = (k_bT)^{-1}$ is the inverse temperature of the environment, $\Phi(\mathbf{x})$ is the free energy of microstate \mathbf{x} (for states with no internal entropy, $\Phi(\mathbf{x})$ is just the energy), and $Z = \sum_{\mathbf{x}} \exp(-\beta\Phi(\mathbf{x}))$ is the partition function. This central result of equilibrium statistical physics has universal validity and its relevance in most areas of physics cannot be overstated. A natural question is whether or not a similar result also holds for non-equilibrium steady states (NESSs), when the system is maintained out of thermal equilibrium by external drives and subjected to constant flows of energy. In this case, one can always write the steady state distribution over microstates as

$$P_{\text{ss}}(\mathbf{x}) = e^{-\mathcal{I}(\mathbf{x})} \quad (2)$$

in terms of the *self-information* $\mathcal{I}(\mathbf{x})$, also known as fluctuating entropy [4, 5]. In order to provide a useful generalization of the Gibbs distribution to NESSs one must relate the self-information $\mathcal{I}(\mathbf{x})$ to measurable physical quantities. This quest has a long history, starting with the seminal contributions of Lebowitz and MacLennan [6–8] and followed by other works [9–15]. However, it still remains an open problem in non-equilibrium statistical physics, since previous formal results are simply not practical in computations, due to the fact that they involve averages over stochastic trajectories.

In this article we prove, for a very general class of open systems displaying a macroscopic limit where a deterministic dynamics emerges, the following fundamental bound on changes of self-information:

$$\Sigma_a \equiv \Sigma + k_b(\mathcal{I}(\mathbf{x}_t) - \mathcal{I}(\mathbf{x}_0)) \geq 0, \quad (3)$$

where $\Sigma = \int_0^t dt' \dot{\Sigma}(\mathbf{x}_{t'})/T$ is the entropy production along a *deterministic trajectory* from microstate \mathbf{x}_0 to microstate \mathbf{x}_t . For example, let us consider the case of chemical reaction networks. The concentrations $\mathbf{x} = (x_1, x_2, \dots)$ of different chemical species reacting in a solution are stochastic quantities, and their evolution is therefore described by a probability distribution $P_t(\mathbf{x})$ at time t . As the volume V of the solution is increased, the distribution $P_t(\mathbf{x})$ becomes strongly localised around the most probable values \mathbf{x}_t for the concentrations at time t , and these values follow a deterministic dynamics that is in general non-linear (given in this case by the chemical rate equations). An analogous situation is encountered in electronic circuits, where the state variables \mathbf{x} are now the voltages at the nodes of a circuit, and the macroscopic limit corresponds to increasing the typical capacitance C of the nodes (as well as the conductivity of the conduction channels connecting pairs of nodes). The remarkable feature of the result in Eq. (3) is that it provides a link between the deterministic dynamics that emerges in the macroscopic limit and the fluctuations observed at steady state. For example, in an electronic circuit powered by voltage sources and working at temperature T , the entropy production rate is $\dot{\Sigma} = -\dot{Q}/T$, where $-\dot{Q}$ is the rate of heat dissipation by the conductive elements of the circuit, that can be easily evaluated at the deterministic level. Then, by Eq. (3), the quantity $-\Sigma/k_b = \int_0^t dt' \dot{Q}(\mathbf{x}_{t'})/(k_bT)$ provides a lower bound to the change of steady state self-information $\mathcal{I}(\mathbf{x}_t) - \mathcal{I}(\mathbf{x}_0)$ along a trajectory. To arrive at our main result in Eq. (3) we consider stochastic systems with a well defined macroscopic limit in which the self-information $\mathcal{I}(x)$ can be shown to be extensive, and Eq. (3) is strictly valid in that limit. However, as we also show, our results can be applied to micro or mesoscopic systems whenever sub-extensive contributions to $\mathcal{I}(x)$ can be neglected.

We interpret our result as an emergent second law of thermodynamics, that is stronger than the usual second law $\Sigma \geq 0$. This last inequality is recovered from Eq.

(3) by considering the fact that $\Delta\mathcal{I} = \mathcal{I}(\mathbf{x}_t) - \mathcal{I}(\mathbf{x}_0) \leq 0$ (to dominant order in the macroscopic limit, the steady state self-information is a Lyapunov function of the deterministic dynamics [16]). In addition to its conceptual value, our result offers a practical tool to approximate or bound non-equilibrium distributions, that can typically only be accessed via stochastic numerical methods (for example the Gillespie algorithm). In contrast, Eq. (3) only requires to know the deterministic dynamics of the system, which is directly given by the well known network analysis techniques commonly applied in electronic circuits and chemical reaction networks. Furthermore, the inequality in Eq. (3) is saturated close to equilibrium, leading to a powerful linear response theory [17]. As an example, we apply our results to a realistic model of non-equilibrium electronic memory: the normal implementation of SRAM (static random access memory) cells in CMOS (complementary metal-oxide-semiconductor) technology. These memories have a non-equilibrium phase transition from a monostable phase to a bistable phase that allows the storage of a bit of information. As we will see, the transition is well captured by Eq. (3), which also allows to bound the probability of fluctuations around the deterministic fixed points. Finally, we show that a general coarse-graining procedure generates equivalent models with minimal entropy production, and that in this way the bound in Eq. (3) becomes tighter. When applied to the CMOS memory, this improved bound enables the full reconstruction of the steady state distribution arbitrarily away from equilibrium.

II. BASIC SETUP

To obtain Eq. (3) we consider stochastic systems described by autonomous Markov jump processes. Thus, let $\{\mathbf{n} \in \mathbb{N}^k\}$ be the set of possible states of the system, and $\lambda_\rho(\mathbf{n})$ be the rates at which jumps $\mathbf{n} \rightarrow \mathbf{n} + \Delta_\rho$ occur, for $\rho = \pm 1, \pm 2, \dots$ and $\Delta_{-\rho} = -\Delta_\rho$ (ρ indexes a possible jump and Δ_ρ is the corresponding change in the state). Each state has energy $E(\mathbf{n})$ and internal entropy $S(\mathbf{n})$. Thermodynamic consistency is introduced by the *local detailed balance* (LDB) condition [18, 19]. It relates the forward and backward jump rates of a given transition with the associated entropy production:

$$\sigma_\rho = \log \frac{\lambda_\rho(\mathbf{n})}{\lambda_{-\rho}(\mathbf{n} + \Delta_\rho)} = -\beta [\Phi(\mathbf{n} + \Delta_\rho) - \Phi(\mathbf{n}) - W_\rho(\mathbf{n})]. \quad (4)$$

In the previous equation, $\Phi(\mathbf{n}) = E(\mathbf{n}) - TS(\mathbf{n})$ is the free energy of state \mathbf{n} , and $W_\rho(\mathbf{n})$ is the non-conservative work provided by external sources during the transition. For simplicity, we have considered isothermal conditions at inverse temperature $\beta = (k_b T)^{-1}$, and therefore the system is taken away from equilibrium by the external work sources alone. More general situations in which a system interacts with several reservoirs at dif-

ferent temperatures can be treated in the same way, this time in terms of a Massieu potential taking the place of $\beta\Phi(\mathbf{n})$ [18]. Important classes of systems accepting the previous description are chemical reaction networks and electronic circuits, which are powered by chemical or electrostatic potential differences, respectively. Note that, by energy conservation, the heat provided by the environment during transition $\mathbf{n} \rightarrow \mathbf{n} + \Delta_\rho$ is $Q_\rho(\mathbf{n}) = E(\mathbf{n} + \Delta_\rho) - E(\mathbf{n}) - W_\rho(\mathbf{n})$, and therefore $k_b\sigma_\rho = -Q_\rho(\mathbf{n})/T + S(\mathbf{n} + \Delta_\rho) - S(\mathbf{n})$.

The probability distribution $P_t(\mathbf{n})$ over the states of the system at time t evolves according to the master equation

$$\partial_t P_t(\mathbf{n}) = \sum_\rho [\lambda_\rho(\mathbf{n} - \Delta_\rho) P_t(\mathbf{n} - \Delta_\rho) - \lambda_\rho(\mathbf{n}) P_t(\mathbf{n})]. \quad (5)$$

From the master equation and the LDB conditions one can derive the energy balance

$$d_t \langle E \rangle = \langle \dot{W} \rangle + \langle \dot{Q} \rangle, \quad (6)$$

and the usual version of the second law:

$$\begin{aligned} \dot{\Sigma} &= \dot{\Sigma}_e + d_t \langle S \rangle \\ &= \frac{k_b}{2} \sum_{\rho, \mathbf{n}} (j_\rho(\mathbf{n}) - j_{-\rho}(\mathbf{n} + \Delta_\rho)) \log \frac{j_\rho(\mathbf{n})}{j_{-\rho}(\mathbf{n} + \Delta_\rho)} \geq 0, \end{aligned} \quad (7)$$

where $j_\rho(\mathbf{n}) = \lambda_\rho(\mathbf{n}) P_t(\mathbf{n})$ is the current associated to transition ρ . In the previous equations, $\langle S \rangle = \sum_{\mathbf{n}} P_t(\mathbf{n}) (S(\mathbf{n}) - k_b \log(P_t(\mathbf{n})))$ is the entropy of the system, $\langle E \rangle = \sum_{\mathbf{n}} E(\mathbf{n}) P_t(\mathbf{n})$ is the average energy, and $\dot{\Sigma}_e$ is the entropy flow rate, given by

$$T \dot{\Sigma}_e = -\langle \dot{Q} \rangle = -\sum_{\rho, \mathbf{n}} Q_\rho(\mathbf{n}) j_\rho(\mathbf{n}) \quad (8)$$

where we also defined the heat rate $\langle \dot{Q} \rangle$ (the work rate $\langle \dot{W} \rangle$ is analogously defined as $\langle \dot{W} \rangle = \sum_{\rho, \mathbf{n}} W_\rho(\mathbf{n}) j_\rho(\mathbf{n})$). Finally, Eq. (7) can be also expressed as:

$$T \dot{\Sigma} = -d_t \langle F \rangle + \langle \dot{W} \rangle \geq 0 \quad (9)$$

where $\langle F \rangle = \langle E \rangle - T \langle S \rangle$ is the non-equilibrium free energy.

Adiabatic/non-adiabtic decomposition – If the support of $P_t(\mathbf{n})$ can be restricted to a finite subspace of the state space, the Perron-Frobenius theorem states that the master equation in Eq. (5) has a unique steady state $P_{ss}(\mathbf{n})$. Once the steady state is attained, the entropy production rate $\dot{\Sigma}$ matches the entropy flow rate $\dot{\Sigma}_e$. An interesting decomposition of the entropy production rate can be obtained by considering the relative entropy $D = \sum_{\mathbf{n}} P_t(\mathbf{n}) \log(P_t(\mathbf{n})/P_{ss}(\mathbf{n}))$ between the instantaneous distribution $P_t(\mathbf{n})$ and the steady state distribution $P_{ss}(\mathbf{n})$. Then, it is possible to show that $\dot{\Sigma} = \dot{\Sigma}_a + \dot{\Sigma}_{na}$, where

$$\dot{\Sigma}_a = \frac{k_b}{2} \sum_{\rho, \mathbf{n}} (j_\rho(\mathbf{n}) - j_{-\rho}(\mathbf{n} + \Delta_\rho)) \log \frac{j_\rho^{ss}(\mathbf{n})}{j_{-\rho}^{ss}(\mathbf{n} + \Delta_\rho)}, \quad (10)$$

and

$$\begin{aligned}\dot{\Sigma}_{\text{na}} &= \frac{k_b}{2} \sum_{\rho, \mathbf{n}} (j_\rho(\mathbf{n}) - j_{-\rho}(\mathbf{n} + \Delta_\rho)) \log \frac{P_t(\mathbf{n}) P_{\text{ss}}(\mathbf{n} + \Delta_\rho)}{P_{\text{ss}}(\mathbf{n}) P_t(\mathbf{n} + \Delta_\rho)} \\ &= -k_b d_t D\end{aligned}\quad (11)$$

are the *adiabatic* and *non-adiabatic* contributions to the entropy production rate $\dot{\Sigma}$, respectively. In Eq. (10) we have introduced the steady state probability currents $j_\rho^{\text{ss}}(\mathbf{n}) = \lambda_\rho(\mathbf{n}) P_{\text{ss}}(\mathbf{n})$. The non-adiabatic contribution $\dot{\Sigma}_{\text{na}}$ is related to the relaxation of the system towards the steady state, since it vanishes when the steady state is reached. This is further evidenced by the identity in the second line of Eq. (11): a reduction in the relative entropy between $P_t(\mathbf{n})$ and $P_{\text{ss}}(\mathbf{n})$ leads to a positive non-adiabatic entropy production. The adiabatic contribution $\dot{\Sigma}_{\text{a}}$ corresponds to the dissipation of ‘housekeeping heat’ [20, 21], and at steady state matches the entropy flow rate $\dot{\Sigma}_e$. An important property of the previous decomposition is that both contributions are individually positive: $\dot{\Sigma}_{\text{a}} \geq 0$ and $\dot{\Sigma}_{\text{na}} \geq 0$ [22–25]. Thus, the last inequality and the second line in Eq. (11) imply that the relative entropy D decreases monotonically, and since D is positive by definition, it is a Lyapunov function for the stochastic dynamics.

Macroscopic limit – In the following we will assume the existence of a scale parameter Ω controlling the size of the system in question. For example, Ω can be taken to be the volume V of the solution in well-mixed chemical reaction networks, or the typical value C of capacitance in the case of electronic circuits (see the example below). In addition, we will assume that for large Ω i) that the typical values of the density $\mathbf{x} \equiv \mathbf{n}/\Omega$ are intensive, ii) that the internal energy and entropy functions $E(\Omega\mathbf{x})$ and $S(\Omega\mathbf{x})$ are extensive, and iii) that the transition rates $\lambda_\rho(\Omega\mathbf{x})$ are also extensive. Under those conditions, the probability distribution $P_t(\mathbf{x})$ satisfies a large deviations (LD) principle [17, 26, 27]:

$$P_t(\mathbf{x}) \asymp e^{-\Omega I_t(\mathbf{x})}, \quad (12)$$

which just means that the limit $I_t(\mathbf{x}) \equiv \lim_{\Omega \rightarrow \infty} -\log(P_t(\mathbf{x}))/\Omega$ is well defined. Then, $I_t(\mathbf{x})$ is a positive, time-dependent ‘rate function’, since it gives the rate at which the probability of fluctuation \mathbf{x} decays with the scale. Note that, by Eq. (12), the steady state self-information introduced in Eq. (2) satisfies $\mathcal{I}(\mathbf{x}) = \Omega I_{\text{ss}}(\mathbf{x})$ to dominant order in the macroscopic limit. In other words, the large deviations principle states that the instantaneous self-information $\mathcal{I}_t(\mathbf{x}) \equiv -\log(P_t(\mathbf{x}))$ is an extensive quantity [26], and we can think of the rate function as the self-information density. Thus, in the following we will consider the ansatz $P_t(\mathbf{x}) = e^{-\Omega I_t(\mathbf{x})}/Z_t$, with $Z_t \equiv \sum_{\mathbf{x}} e^{-\Omega I_t(\mathbf{x})}$, as an approximation to the actual time-dependent distribution. This amounts to neglecting sub-extensive contributions to the instantaneous self-information. As explained below, $I_t(\mathbf{x})$ takes its minimum value $I_t(\mathbf{x}_t) = 0$ at

the deterministic trajectory \mathbf{x}_t , which is equivalent to $P_t(\mathbf{x}) = \delta(\mathbf{x} - \mathbf{x}_t)$ for $\Omega \rightarrow \infty$. Plugging the previous ansatz in the master equation of Eq. (5) we note that $\lambda_\rho(\mathbf{x} - \Delta_\rho/\Omega) P_t(\mathbf{x} - \Delta_\rho/\Omega) \simeq \lambda_\rho(\mathbf{x}) P_t(\mathbf{x}) e^{\Delta_\rho \cdot \nabla I_t(\mathbf{x})}$ to dominant order in $\Omega \rightarrow \infty$. Noting also that $\log(Z_t)$ is sub-extensive, it is possible to see that $I_t(\mathbf{x})$ evolves according to

$$\partial_t I_t(\mathbf{x}) = \sum_{\rho} \omega_\rho(\mathbf{x}) \left[1 - e^{\Delta_\rho \cdot \nabla I_t(\mathbf{x})} \right], \quad (13)$$

where $\omega_\rho(\mathbf{x}) \equiv \lim_{\Omega \rightarrow \infty} \lambda_\rho(\Omega\mathbf{x})/\Omega$ are the scaled jump rates [17, 28]. In a similar way, in the macroscopic limit the LDB conditions in Eq. (4) take the form

$$\log \frac{\omega_\rho(\mathbf{x})}{\omega_{-\rho}(\mathbf{x})} = -\beta [\Delta_\rho \cdot \nabla \phi(\mathbf{x}) - W_\rho(\mathbf{x})], \quad (14)$$

in terms of the free energy density $\phi(\mathbf{x}) \equiv \lim_{\Omega \rightarrow \infty} \Phi(\Omega\mathbf{x})/\Omega$ (internal energy and entropy densities $\epsilon(\mathbf{x})$ and $s(\mathbf{x})$ satisfying $\phi(\mathbf{x}) = \epsilon(\mathbf{x}) - Ts(\mathbf{x})$ can be defined in the same way). For the work contributions in Eq. (14) we are abusing notation by writing $W_\rho(\mathbf{x}) = \lim_{\Omega \rightarrow \infty} W_\rho(\mathbf{n} = \Omega\mathbf{x})$. Note that we assume that work contributions are intensive. This is justified since they are given by the product of two intensive quantities: a thermodynamic force (for example a potential difference), and the change in a conserved quantity (mass, charge, etc) *during a single jump* [29]. However, note also that the work rate $\langle \dot{W} \rangle$ will be extensive in general due to the extensivity of the transition rates.

Many classes of systems satisfy the previous scaling assumptions besides the examples already mentioned. Additional examples include non-equilibrium many-body problems like the driven Potts model [30, 31], reaction-diffusion models [32, 33], and asymmetric exclusion processes [32, 34].

From Eq. (12) we see that as Ω is increased, $P_t(\mathbf{x})$ is increasingly localised around the minimum of the rate function $I_t(\mathbf{x})$, which is the most probable value. Also, deviations from that typical state are exponentially suppressed in Ω . Thus, the limit $\Omega \rightarrow \infty$ is a macroscopic low-noise limit where a deterministic dynamic emerges. In fact, from Eq. (13) one can show that the evolution of the minima \mathbf{x}_t of $I_t(\mathbf{x})$ is ruled by the closed non-linear differential equations

$$d_t \mathbf{x}_t = \mathbf{u}(\mathbf{x}_t) \quad \text{with} \quad \mathbf{u}(\mathbf{x}) = \sum_{\rho > 0} i_\rho(\mathbf{x}) \Delta_\rho, \quad (15)$$

where $i_\rho(\mathbf{x}) \equiv \omega_\rho(\mathbf{x}) - \omega_{-\rho}(\mathbf{x})$ are the scaled deterministic currents [17]. The vector field $\mathbf{u}(\mathbf{x})$ corresponds to the deterministic drift in state space. For chemical reaction networks the dynamical equations in Eq. (15) are the chemical rate equations, while for electronic circuits they are provided by regular circuit analysis.

In the following section we obtain bounds for the steady state rate function $I_{\text{ss}}(\mathbf{x})$, that according to Eq.

(13) satisfies:

$$0 = \sum_{\rho} \omega_{\rho}(\mathbf{x}) \left[1 - e^{\Delta_{\rho} \cdot \nabla I_{\text{ss}}(\mathbf{x})} \right]. \quad (16)$$

III. EMERGENT SECOND LAW

The positivity of the adiabatic and non-adiabatic contributions to the entropy production, $\dot{\Sigma}_{\text{a}} \geq 0$ and $\dot{\Sigma}_{\text{na}} \geq 0$, in addition to the usual second law $\dot{\Sigma} \geq 0$, have been called the ‘three faces of the second law’ [23]. In [28], the inequality $\dot{\Sigma}_{\text{na}} = -k_b d_t D \geq 0$ was put forward as an ‘emergent’ second law. There, $\mathcal{F} = k_b D$ was interpreted as an alternative non-equilibrium free energy, with a balance equation $d_t \mathcal{F} = \Sigma_{\text{a}} - \dot{\Sigma} \leq 0$ (note the analogy with Eq. (9)). Then, the adiabatic contribution $\dot{\Sigma}_{\text{a}}$ was interpreted as an energy input, which at steady state balances the dissipation $\dot{\Sigma}$. Although this point of view is compelling, it is hindered by the fact that there is no clear interpretation of $\dot{\Sigma}_{\text{a}}$ away from the steady state, that would allow to compute this quantity in terms of actual physical currents. In this work we take the other possible road, and investigate the interpretation and consequences of $\dot{\Sigma}_{\text{a}} \geq 0$. We begin by rewriting Eq. (10) using the LDB conditions of Eq. (4) and the definition of \mathcal{I} in Eq. (2), obtaining:

$$\dot{\Sigma}_{\text{a}} = \dot{\Sigma} + k_b d_t \langle \mathcal{I} \rangle - d_t \langle S_{\text{sh}} \rangle \geq 0, \quad (17)$$

where we have defined $\langle \mathcal{I} \rangle = \sum_{\mathbf{n}} \mathcal{I}(\mathbf{n}) P_t(\mathbf{n})$ as the average of the steady state self-information $\mathcal{I}(\mathbf{n}) = -\log(P_{\text{ss}}(\mathbf{n}))$ and $\langle S_{\text{sh}} \rangle = -k_b \sum_{\mathbf{n}} P_t(\mathbf{n}) \log(P_t(\mathbf{n}))$ as the Shannon contribution to the system entropy, computed over the instantaneous distribution. Eq. (17) has been already obtained in [22–24], although it was not explicitly written in terms of the self-information \mathcal{I} . It is important to note that $\langle S_{\text{sh}} \rangle$ is sub-extensive in Ω (according to Eq. (12), it grows as $\log(\Omega)$), and therefore can be neglected in the macroscopic limit. Thus, changes in average self-information can be bounded by the entropy production, that can in turn be computed or measured in terms of actual energy and entropy flows (see Eqs. (7) and (8)). However, the result in Eq. (17) is not yet in a useful form, since the average $\langle \mathcal{I} \rangle$ does not depend only on $\mathcal{I}(\mathbf{n})$, the unknown quantity we are interested in, but also on the instantaneous distribution $P_t(\mathbf{n})$, that is also typically unknown. This issue is circumvented in the macroscopic limit, since in that case $P_t(\mathbf{x})$ is strongly localised around the deterministic values \mathbf{x}_t , and therefore $\langle \mathcal{I} \rangle \simeq \Omega I_{\text{ss}}(\mathbf{x}_t)$ to dominant order in $\Omega \rightarrow \infty$. Thus, in the same limit, Eq. (17) for the adiabatic entropy production rate $\dot{\Sigma}_{\text{a}}$ reduces to

$$\dot{\sigma}_{\text{a}}(\mathbf{x}_t) = \dot{\sigma}(\mathbf{x}_t) + k_b d_t I_{\text{ss}}(\mathbf{x}_t) \geq 0, \quad (18)$$

where we have defined $\dot{\sigma}(\mathbf{x}_t) = \lim_{\Omega \rightarrow \infty} \dot{\Sigma}/\Omega$ as the scaled macroscopic limit of the entropy production rate

($\dot{\sigma}_{\text{a}}(\mathbf{x}_t)$ is defined in a similar way). Eq. (18) is a more rigorous version of our central result in Eq. (3), which is obtained by integrating Eq. (18) along deterministic trajectories (satisfying Eq. (15)) and multiplying by the scale factor. It is also useful to write down the first and second laws in the macroscopic limit. The energy balance in Eq. (6) reduces to

$$d_t \epsilon(\mathbf{x}_t) = \mathbf{u}(\mathbf{x}_t) \cdot \nabla \epsilon(\mathbf{x}_t) = \dot{w}(\mathbf{x}_t) + \dot{q}(\mathbf{x}_t), \quad (19)$$

where the scaled heat and work rates for state \mathbf{x} are defined as $\dot{q}(\mathbf{x}) = \sum_{\rho>0} i_{\rho}(\mathbf{x}) Q_{\rho}(\mathbf{x})$ and $\dot{w}(\mathbf{x}) = \sum_{\rho>0} i_{\rho}(\mathbf{x}) W_{\rho}(\mathbf{x})$, respectively. Finally, again neglecting the sub-extensive Shannon contribution $\langle S_{\text{sh}} \rangle$, the second law in Eq. (7) reduces to

$$\begin{aligned} \dot{\sigma}(\mathbf{x}_t) &= -\dot{q}(\mathbf{x}_t)/T + d_t s(\mathbf{x}_t) \\ &= k_b \sum_{\rho>0} (\omega_{\rho}(\mathbf{x}_t) - \omega_{-\rho}(\mathbf{x}_t)) \log \frac{\omega_{\rho}(\mathbf{x}_t)}{\omega_{-\rho}(\mathbf{x}_t)} \geq 0. \end{aligned} \quad (20)$$

Linear response regime – We will now show that to first order in the work contributions $W_{\rho}(\mathbf{x})$ the inequality in Eq. (18) is saturated. In first place we rewrite Eq. (18) using the macroscopic first and second laws in Eqs. (19) and (20):

$$\dot{\sigma}_{\text{a}}(\mathbf{x}_t)/k_b = \mathbf{u}(\mathbf{x}_t) \cdot \nabla (I_{\text{ss}}(\mathbf{x}) - \beta \phi(\mathbf{x}))|_{\mathbf{x}=\mathbf{x}_t} + \beta \dot{w}(\mathbf{x}_t), \quad (21)$$

where we also used $\phi(\mathbf{x}) = \epsilon(\mathbf{x}) - T s(\mathbf{x})$ and that $d_t F(\mathbf{x}_t) = \mathbf{u}(\mathbf{x}_t) \cdot \nabla F(\mathbf{x}_t)$ for any function $F(\mathbf{x})$. Secondly, we note that in detailed balanced settings (i.e., if $W_{\rho}(\mathbf{x}) = 0 \forall \rho, \mathbf{x}$) the steady state rate function is just $I_{\text{ss}}(\mathbf{x}) = \beta \phi(\mathbf{x})$ (up to a constant), in accordance to the Gibbs distribution (this follows from Eqs. (14) and (16)). Thus, the difference $g(\mathbf{x}) \equiv I_{\text{ss}}(\mathbf{x}) - \beta \phi(\mathbf{x})$ appearing in Eq. (18) quantifies the deviations from thermal equilibrium. Expanding Eq. (16) to first order in $W_{\rho}(\mathbf{x})$ and $g(\mathbf{x})$, it can be shown that

$$\mathbf{u}^{(0)}(\mathbf{x}) \cdot \nabla g(\mathbf{x}) = -\beta \dot{w}^{(0)}(\mathbf{x}) + \mathcal{O}(W_{\rho}^2), \quad (22)$$

where $\mathbf{u}^{(0)}(\mathbf{x}) = \sum_{\rho>0} i_{\rho}^{(0)}(\mathbf{x}) \Delta_{\rho}$ and $\dot{w}^{(0)}(\mathbf{x}) = \sum_{\rho>0} i_{\rho}^{(0)}(\mathbf{x}) W_{\rho}(\mathbf{x})$ are the lowest-order deterministic drift and work rate, respectively [17]. These are defined in terms of the detailed balanced deterministic currents $i_{\rho}^{(0)}(\mathbf{x}) = \omega_{\rho}^{(0)}(\mathbf{x}) - \omega_{-\rho}^{(0)}(\mathbf{x})$ constructed from the scaled transition rates evaluated at $W_{\rho}(\mathbf{x}) = 0$ that, according to the LDB conditions of Eq. (14), satisfy $\log(\omega_{\rho}^{(0)}(\mathbf{x})/\omega_{-\rho}^{(0)}(\mathbf{x})) = -\beta \Delta_{\rho} \cdot \nabla \phi(\mathbf{x})$. Comparing the result of Eq. (22) with Eq. (21), we see that $\dot{\Sigma}_{\text{a}} = 0$ to linear order in $W_{\rho}(\mathbf{x})$. Then, in the linear response regime we can write:

$$\begin{aligned} I_{\text{ss}}(\mathbf{x}_t) - I_{\text{ss}}(\mathbf{x}_0) &\simeq - \int_0^t dt' \dot{\sigma}^{(0)}(\mathbf{x}_{t'})/k_b \\ &= \beta \left[\phi(\mathbf{x}_t) - \phi(\mathbf{x}_0) - \int_0^t dt' \dot{w}^{(0)}(\mathbf{x}_{t'}) \right]. \end{aligned} \quad (23)$$

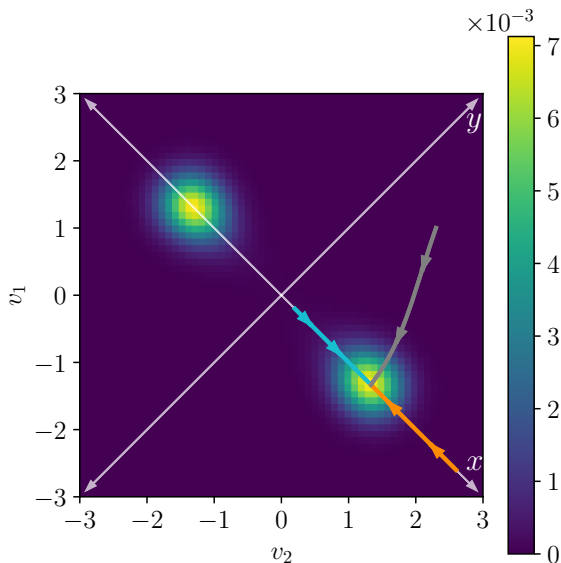


FIG. 1: Exact steady state distribution for $V_{\text{dd}} = 1.4$ and $v_e = 0.1$. Also shown are three deterministic trajectories for the same parameters.

where the integration is performed along trajectories solving the detailed balanced deterministic dynamics $d_t \mathbf{x}_t = \mathbf{u}^{(0)}(\mathbf{x}_t)$.

IV. EXAMPLE

In order to illustrate our results we will consider the model of a low-power CMOS memory cell developed in [35, 36], that we review in the Supplementary Material. This model involves two CMOS inverters connected in a loop, and each inverter is composed of two MOS transistors. There are two degrees of freedom: voltages v_1 and v_2 , that can take values spaced by the elementary voltage $v_e = q_e/C$, where q_e is the positive electron charge and C is a value of capacitance that increases with the scale of the MOS transistors. Thus, in this context the scale parameter can be taken to be $\Omega = V_T/v_e$, where $V_T = k_b T/q_e$ is the thermal voltage. In the following all voltages will be expressed in units of V_T . Figure 1 shows a typical steady state distribution in the bistable phase, and three different deterministic trajectories. The logical state of the memory is codified in the sign of the variable $x = v_1 - v_2$. The rate function $I_{\text{ss}}(x)$ along the x axis in Figure 1 can be computed exactly [36]:

$$I_{\text{ss}}(x) = x^2 + 2xV_{\text{dd}} + \frac{2n}{n+2} [L(x, V_{\text{dd}}) - L(x, -V_{\text{dd}})], \quad (24)$$

where V_{dd} is the powering voltage that takes the memory out of thermal equilibrium, $L(x, V_{\text{dd}}) =$

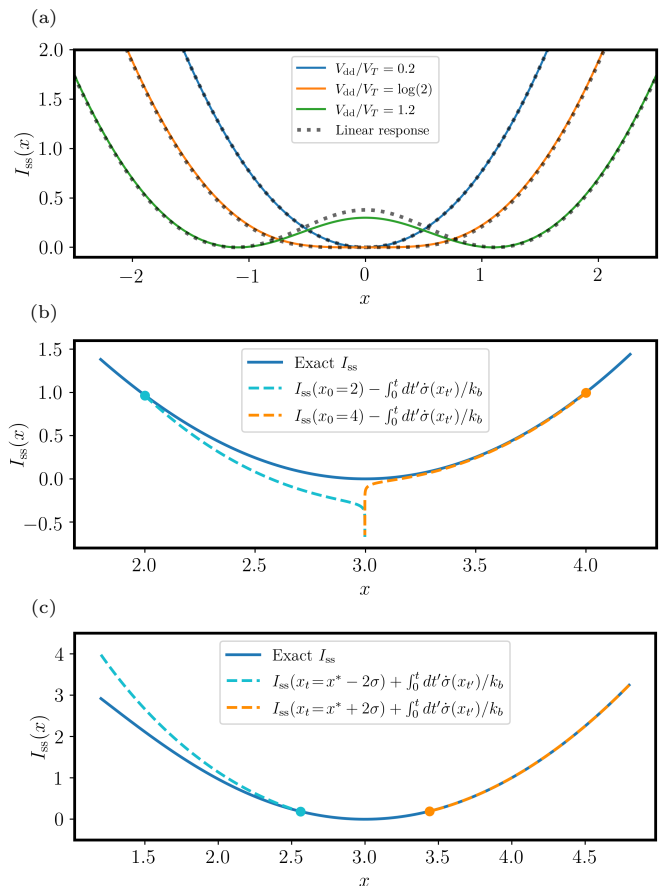


FIG. 2: (a) Rate function $I_{\text{ss}}(x)$ for different values of the powering voltage V_{dd} . We also compare $I_{\text{ss}}(x)$ with the linear response approximation obtained from Eq. (23) for $V_{\text{dd}} = 1.2$. (b) Illustration of the bound to $I(x_t)$ in Eq. (18) for two different deterministic trajectories starting at $x_0 = 2$ and $x_0 = 4$ ($V_{\text{dd}} = 3$) (c) Bound to $I(x_0)$ for a fixed x_t according to Eq. (18), for $x_t = x^* \pm 2\delta$ ($\delta = 1/\sqrt{2\Omega}$, $\Omega = 10$, and $V_{\text{dd}} = 3$).

$\text{Li}_2(-\exp(V_{\text{dd}} + x(1 + 2/n)))$, and $\text{Li}_2(\cdot)$ is the polylogarithm function of second order. Also, $n \geq 1$ is a parameter that characterizes the transistors (the slope factor), and that will be fixed to $n = 1$ in the following. In the Supplementary Material we show that the rate function in Eq. (24) provides an essentially exact description of the steady state distribution for scale parameters as low as $\Omega = 10$ (i.e., states with at most tens of electrons are appreciably populated). Thus, sub-extensive contributions to the self-information can be safely neglected in this case, even away from the strict macroscopic limit.

In Figure 2-(a) we show that there is a non-equilibrium transition from a monostable phase into the bistable phase that allows the storage of a bit of information, occurring at the critical powering voltage $V_{\text{dd}}^* = \ln(2)$. We also compare the exact rate function in Eq. (24) with the linear response approximation obtained from Eq. (23) for different powering voltages. Remarkably, despite it is

only expected to be valid close to equilibrium, the linear response approximation captures the transition to bistability and continues to be a reasonable approximation well into the bistable phase. The reason is that in this case the second order non-equilibrium correction vanishes (as can be checked by expanding Eq. (24) in V_{dd}), and therefore the linear response approximation is actually valid up to order V_{dd}^3 .

In Figure 2-(b) the exact rate function $I_{\text{ss}}(x_t)$ along a deterministic trajectory x_t is compared with the lower bound $I_{\text{ss}}(x_0) - \int_0^t dt' \dot{\sigma}(x_{t'})/k_b$, for two different trajectories starting at $x_0 = 2$ and $x_0 = 4$, with $y_0 = 0$ in both cases (as shown in Figure 1, deterministic trajectories initialized in the x axis remain in it). In both cases the trajectory x_t approaches the fixed point $x^* \simeq V_{\text{dd}} = 3$. We see that $I_{\text{ss}}(x_0) - \int_0^t dt' \dot{\sigma}(x_{t'})/k_b$ is indeed a lower bound to $I_{\text{ss}}(x_t)$, in accordance with Eq. (3). Note that this bound diverges when the trajectory approaches the fixed point x^* . The reason is that once $x_t \simeq x^*$, the entropy production $\int_0^t dt' \dot{\sigma}(x_{t'})$ just continuously integrates the steady state heat dissipation rate $-\dot{q}(x^*)$ (see Eq. (20)). The linear response approximation avoids this issue since the lowest-order work rate $\dot{w}^{(0)}(x)$ vanishes at the equilibrium fixed point (see Eq. (23)). The divergence can be also avoided by the coarse-graining procedure discussed in the next section. Alternatively, Eq. (3) can be considered an upper bound to $I(x_0)$ for a fixed final point x_t . This is shown in Figure 2-(c), for final points $x_t = x^* \pm 2\delta$, where $\delta = 1/\sqrt{2\Omega}$ estimates the variance of the fluctuations around the fixed point.

The fact that in Figures 2-(b, c) the bounds are much tighter to one side of the fixed point than the other can be traced back to the different speeds at which the fixed point is approached. To show this, in Figure 3 we have plotted the entropy production rate $\dot{\sigma}$ and the speed $|dx/dt|$ as a function of x for $V_{\text{dd}} = 3$. In Figure 3-(a) we see that $\dot{\sigma}$ is minimized close to the deterministic fixed points (this is a design feature of CMOS devices, in order to minimize the static power consumption, which is however not zero). Also, we see that $\dot{\sigma}$ is actually lower to the left of the fixed point at $x \simeq 3$ than to the right. However, in Figure 3-(b) we see that the speed dx/dt at which the fixed point is approached is also lower to the left side, resulting in a larger total entropy production $\int_0^t dt' \dot{\sigma}(x_{t'}) = \int_{x_0}^{x_t} dx \dot{\sigma}(x)/(dx/dt)$, and a looser bound in Figures 2-(b, c).

V. TIGHTENING THE BOUND

Our main result in Eq. (3) allows to obtain information about the steady state fluctuations by just measuring the physical entropy production along deterministic trajectories. However, if we consider the mathematical problem of bounding the steady state fluctuations given the transition rates $\lambda_\rho(\mathbf{n})$, then the full power of our result is achieved by considering a ‘coarse-grained’ en-

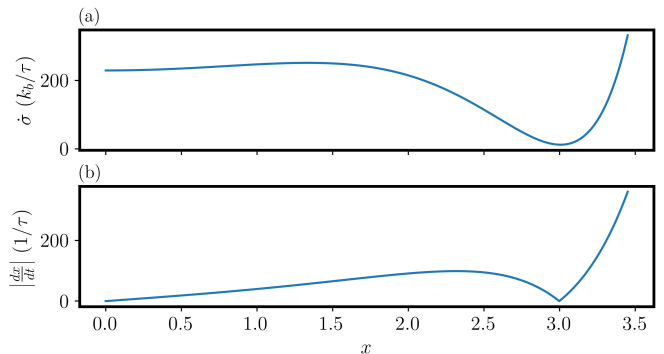


FIG. 3: (a) Deterministic entropy production rate $\dot{\sigma}$, and (b) deterministic speed $|dx/dt|$ as a function of x for $V_{\text{dd}} = 3$ (see the Supplementary Material for the definition of the timescale τ).

trophy production that is in general a lower bound to the actual physical one, as we now explain. In first place we notice that different sets of transition rates $\{\lambda_\rho(\mathbf{n})\}$ might lead to the same master equation (Eq. (5)) and consequently the same steady state and emerging deterministic dynamics (Eq. (15)), while giving rise to different entropy production rates (Eq. (7)). This is due to the fact that the entropy production depends on how a given stochastic dynamics is split into thermodynamically distinct processes, each of them satisfying a different LDB condition. In particular, the entropy production is not invariant under coarse-graining of the transition rates [23, 37]. Specifically, consider that we lump together all transitions going from state \mathbf{n} to state $\mathbf{n} + \tilde{\Delta}_\rho$ into a single transition with rate

$$\tilde{\lambda}_\rho(\mathbf{n}) \equiv \sum_{\rho'/\tilde{\Delta}_{\rho'}=\tilde{\Delta}_\rho} \lambda_{\rho'}(\mathbf{n}). \quad (25)$$

In this way, the jump vectors $\{\tilde{\Delta}_\rho\}$ associated to the coarse-grained rates $\tilde{\lambda}_\rho(\mathbf{n})$ are all distinct ($\tilde{\Delta}_\rho \neq \tilde{\Delta}_{\rho'}$ if $\rho \neq \rho'$). It is easy to check that rates $\{\tilde{\lambda}_\rho(\mathbf{n})\}$ and $\{\lambda_\rho(\mathbf{n})\}$ lead to the same master equation. However, the entropy production rate $\tilde{\Pi}$ corresponding to the rates $\{\tilde{\lambda}_\rho(\mathbf{n})\}$ is always a lower bound of the original one [23]:

$$\tilde{\Pi} = \frac{k_b}{2} \sum_{\rho, \mathbf{n}} (\tilde{j}_\rho(\mathbf{n}) - \tilde{j}_{-\rho}(\mathbf{n} + \tilde{\Delta}_\rho)) \log \frac{\tilde{j}_\rho(\mathbf{n})}{\tilde{j}_{-\rho}(\mathbf{n} + \tilde{\Delta}_\rho)} \leq \dot{\Sigma} \quad (26)$$

An important property of $\tilde{\Pi}$ is that, whenever the emerging deterministic dynamics has fixed point attractors, its macroscopic version $\dot{\pi}(\mathbf{x}_t) \equiv \lim_{\Omega \rightarrow \infty} \tilde{\Pi}/\Omega = \sum_{\rho > 0} (\tilde{\omega}_\rho(\mathbf{x}_t) - \tilde{\omega}_{-\rho}(\mathbf{x}_t)) \log(\tilde{\omega}_\rho(\mathbf{x}_t)/\tilde{\omega}_{-\rho}(\mathbf{x}_t))$ vanishes at the fixed points (see the Supplementary Material for a detailed discussion). Thus, the bound obtained using the entropy production rate $\dot{\pi}$ is free from the divergence as

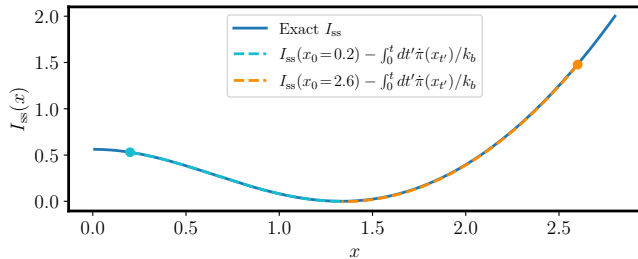


FIG. 4: Illustration of the bound to $I(x_t)$ in Eq. (3) for the cyan and orange trajectories in Figure 1, stating respectively at $x_0 = 0.2$ and $x_0 = 2.6$ ($V_{\text{ad}} = 1.4$).

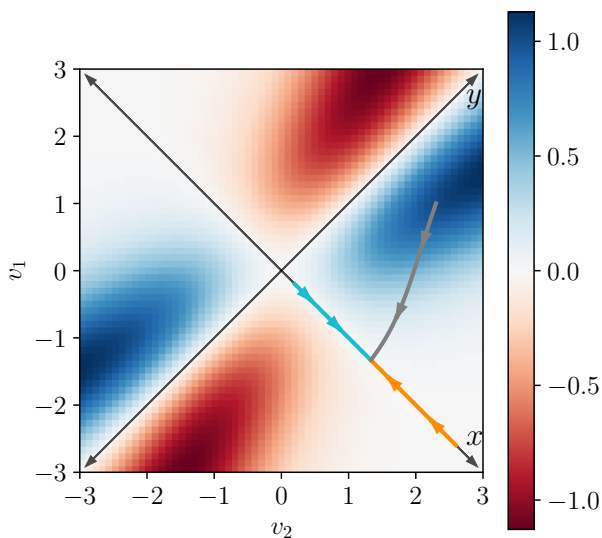


FIG. 5: Vorticity $f(\mathbf{x})$ of the vector field with components $\tilde{\sigma}_\rho(\mathbf{x}) \equiv \log(\tilde{\omega}_\rho(\mathbf{x})/\tilde{\omega}_{-\rho}(\mathbf{x}))$, $\rho = 1, 2$, for the CMOS memory model. The parameters and the displayed deterministic trajectories are the same as in Figure 1.

the fixed point is approached. In the case of the CMOS memory, this is shown in Figure 4 for the two trajectories along the x axis of Figure 1. We see that not only the divergence is avoided, but that the bound matches the exact rate function. This is explained in the following.

Coarse-grained local detailed balance. In analogy with Eq. (14), whenever the log-ratio $\tilde{\sigma}_\rho(\mathbf{x}) \equiv \log(\tilde{\omega}_\rho(\mathbf{x})/\tilde{\omega}_{-\rho}(\mathbf{x}))$ of the scaled coarse-grained rates can be expressed as the gradient of a state function $-\tilde{\phi}(\mathbf{x})$ along the direction $\tilde{\Delta}_\rho$, the steady state rate function will be just $I_{\text{ss}}(\mathbf{x}) = \tilde{\phi}(\mathbf{x})$ (up to a constant). In that case, the system can be considered to be at equilibrium at the coarse-grained level. Under some conditions, one can easily test if $\tilde{\sigma}_\rho(\mathbf{x})$ derives from a gradient by just checking

if the generalized curl $f_{\rho, \rho'}(\mathbf{x}) \equiv \partial_{x_\rho} \tilde{\sigma}_{\rho'}(\mathbf{x}) - \partial_{x_{\rho'}} \tilde{\sigma}_\rho(\mathbf{x})$ vanishes for all ρ, ρ' , and \mathbf{x} (see the Supplementary Material). If that is the case, then the bound in Eq. (18) in terms of the entropy production Π is saturated, and one can fully reconstruct the steady state rate function in terms of the deterministic dynamics.

In the CMOS memory the state space is two dimensional and therefore there is a single curl component $f(\mathbf{x})$, or vorticity. In Figure 5 we show the vorticity $f(\mathbf{x})$ for the same parameters as in Figure 1. We see that the model is genuinely non-equilibrium even at the coarse-grained level. However, we also see that the vorticity vanishes at the x and y axes, which explains why the bound in Figure 4 matches the exact rate function. Finally, we study how the bound in terms of the coarse-grained entropy production rate $\dot{\pi}$ performs for the gray trajectory in Figures 1 and 5, that starts in and goes through areas of non-vanishing vorticity, and thus genuinely out of equilibrium. Since in this case we do not have the exact rate function to compare with, we compare the bound with estimation of the rate function $I_{\text{est}}(\mathbf{x}) = -\log(P_{\text{ss}}(\mathbf{x}))/\Omega$ obtained from the exact steady state distribution. $I_{\text{est}}(\mathbf{x})$ is only defined for the discrete set of voltages v_1 and v_2 that are a multiple of the elementary voltage v_e , and in the comparison we choose the closest values of v_1 and v_2 to the continuous deterministic trajectory \mathbf{x}_t , obtaining an stepwise function. The results are shown in Figure 6. We see that even in this case our bound provides an accurate approximation of the probability distribution. This shows that the emergent second law in terms of the coarse-grained entropy production has the potential to offer a deterministic alternative to Gillespie simulations and spectral methods. As an example, we provide in the Supplementary Material a full reconstruction of the steady state distribution of the CMOS memory.

It is important to note that the bound given by the emergent second law in terms of the mathematical entropy production in Eq. (26) can be applied to any Markov jump process displaying a macroscopic limit, irrespective of whether it represents a thermodynamically consistent stochastic dynamics or not (the only restriction is that for each jump the reverse jump should also be possible). For example, our results can be relevant in stochastic population [38, 39] or gene expression [40, 41] models.

VI. DISCUSSION

For systems accepting a description in terms of Markov jump processes, our results unveil a fundamental connection between the deterministic dynamics that emerges in a macroscopic limit and the non-equilibrium fluctuations at steady state. This is given by an inequality that can be interpreted as an emergent second law. In fact, it is a tighter version of the usual second law, that is saturated in the linear response regime. The practical value of our result lies in the fact that the probability of non-

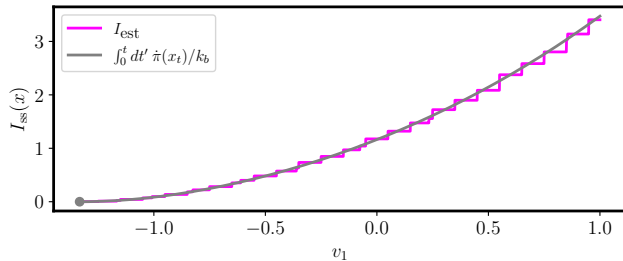


FIG. 6: Comparison of the upper bound to $I_{ss}(\mathbf{x}_0)$ in terms of the coarse-grained entropy production rate $\dot{\pi}$ for the points in the gray trajectory in Figures 1 and 5 with the function $I_{\text{est}}(\mathbf{x}) = -\log(P_{ss}(\mathbf{x}))/\Omega$ obtained from the exact steady state distribution.

equilibrium fluctuations is hard to evaluate, while the deterministic dynamics is directly given by standard methods. The corresponding linear response theory, working at the level of the rate function, was shown in [17] to be highly accurate in some model systems, with a regime of validity beyond that of usual linear response theories. Our result can also be employed in combination with numerical or experimental approaches: once normal or moderately rare fluctuations have been sampled and characterized, Eq. (3) can be used to bound the probability of very rare fluctuations, that otherwise would require

extremely long simulation times. In addition, the refinement of our result by a coarse-graining procedure leads to novel numerical techniques to compute non-equilibrium distributions, that only rely on the deterministic dynamics and thus offer an alternative to stochastic simulations or spectral methods.

As a final comment, we note that the extensivity assumptions defining the macroscopic limit we have considered are a very natural extension of the usual notion of extensivity in equilibrium thermodynamics. The only additional requirements, besides the extensivity of the free energy associated to each state, are the extensivity of the jump rates between different states, and the intensivity of the work contributions. These natural requirements lead to an extensive non-equilibrium self-information, whose dominant contribution is constrained by our emergent second law, and that at equilibrium reduces to the regular extensive free energy.

VII. ACKNOWLEDGMENTS

We acknowledge funding from the INTER project “TheCirco” (INTER/FNRS/20/15074473) and CORE project “NTEC” (C19/MS/13664907), funded by the Fonds National de la Recherche (FNR, Luxembourg), and from the European Research Council, project NanoThermo (ERC-2015-CoGAgreement No. 681456).

-
- [1] Sheldon Goldstein, Joel L Lebowitz, Roderich Tumulka, and Nino Zanghì. Canonical typicality. *Physical review letters*, 96(5):050403, 2006.
 - [2] Sandu Popescu, Anthony J Short, and Andreas Winter. Entanglement and the foundations of statistical mechanics. *Nature Physics*, 2(11):754–758, 2006.
 - [3] Hans-Otto Georgii. *Gibbs Measures and Phase Transitions*. De Gruyter, Berlin, Germany, May 2011.
 - [4] Albert Einstein. Theorie der Opaleszenz von homogenen Flüssigkeiten und Flüssigkeitsgemischen in der Nähe des kritischen Zustandes. *Annalen der Physik*, 338(16):1275–1298, 1910.
 - [5] Udo Seifert. Entropy production along a stochastic trajectory and an integral fluctuation theorem. *Physical review letters*, 95(4):040602, 2005.
 - [6] Joel L Lebowitz and Peter G Bergmann. Irreversible gibbsian ensembles. *Annals of Physics*, 1(1):1–23, 1957.
 - [7] JL Lebowitz. Stationary nonequilibrium gibbsian ensembles. *Physical Review*, 114(5):1192, 1959.
 - [8] James A McLennan Jr. Statistical mechanics of the steady state. *Physical review*, 115(6):1405, 1959.
 - [9] Dmitrii Nikolaevich Zubarev. *Nonequilibrium statistical thermodynamics*. Consultants Bureau, 1974.
 - [10] DN Zubarev. Nonequilibrium statistical operator as a generalization of gibbs distribution for nonequilibrium case. *Cond. Matt. Phys*, 4(7), 1994.
 - [11] Teruhisa S Komatsu and Naoko Nakagawa. Expression for the stationary distribution in nonequilibrium steady states. *Physical review letters*, 100(3):030601, 2008.
 - [12] Christian Maes and Karel Netočný. Rigorous meaning of mcLennan ensembles. *Journal of mathematical physics*, 51(1):015219, 2010.
 - [13] Matteo Colangeli, Christian Maes, and Bram Wynants. A meaningful expansion around detailed balance. *Journal of Physics A: Mathematical and Theoretical*, 44(9):095001, 2011.
 - [14] Abhishek Dhar, Keiji Saito, and Peter Hänggi. Nonequilibrium density-matrix description of steady-state quantum transport. *Physical Review E*, 85(1):011126, 2012.
 - [15] H Ness. Nonequilibrium density matrix for quantum transport: Hershfield approach as a mcLennan-zubarev form of the statistical operator. *Physical Review E*, 88(2):022121, 2013.
 - [16] Hu Gang. Lyapounov function and stationary probability distributions. *Zeitschrift für Physik B Condensed Matter*, 65(1):103–106, 1986.
 - [17] Nahuel Freitas, Gianmaria Falasco, and Massimiliano Esposito. Linear response in large deviations theory: a method to compute non-equilibrium distributions. *New Journal of Physics*, 23(9):093003, Sep 2021.
 - [18] Riccardo Rao and Massimiliano Esposito. Conservation laws shape dissipation. *New Journal of Physics*, 20(2):023007, feb 2018.
 - [19] Christian Maes. Local detailed balance. *SciPost Phys. Lect. Notes*, 32:1–17, 2021.
 - [20] Takahiro Hatano and Shin-ichi Sasa. Steady-state thermodynamics of langevin systems. *Physical review letters*, 86(16):3463, 2001.

- [21] Thomas Speck and Udo Seifert. Integral fluctuation theorem for the housekeeping heat. *Journal of Physics A: Mathematical and General*, 38(34):L581, 2005.
- [22] Massimiliano Esposito, Upendra Harbola, and Shaul Mukamel. Entropy fluctuation theorems in driven open systems: Application to electron counting statistics. *Phys. Rev. E*, 76(3):031132, Sep 2007.
- [23] Massimiliano Esposito and Christian Van den Broeck. Three faces of the second law. I. Master equation formulation. *Phys. Rev. E*, 82(1):011143, Jul 2010.
- [24] Hao Ge and Hong Qian. Physical origins of entropy production, free energy dissipation, and their mathematical representations. *Phys. Rev. E*, 81(5):051133, May 2010.
- [25] Riccardo Rao and Massimiliano Esposito. Detailed fluctuation theorems: A unifying perspective. *Entropy*, 20(9):635, 2018.
- [26] Hugo Touchette. The large deviation approach to statistical mechanics. *Physics Reports*, 478(1-3):1–69, 2009.
- [27] Hugo Touchette and Rosemary J. Harris. Large deviation approach to nonequilibrium systems. *arXiv*, Oct 2011.
- [28] Hao Ge and Hong Qian. Mesoscopic kinetic basis of macroscopic chemical thermodynamics: A mathematical theory. *Physical Review E*, 94(5):052150, 2016.
- [29] Riccardo Rao and Massimiliano Esposito. Conservation laws shape dissipation. *New Journal of Physics*, 20(2):023007, 2018.
- [30] Tim Herpich, Juzar Thingna, and Massimiliano Esposito. Collective Power: Minimal Model for Thermodynamics of Nonequilibrium Phase Transitions. *Phys. Rev. X*, 8(3):031056, September 2018.
- [31] Tim Herpich, Tommaso Cossetto, Gianmaria Falasco, and Massimiliano Esposito. Stochastic thermodynamics of all-to-all interacting many-body systems. *New Journal of Physics*, 22(6):063005, 2020.
- [32] Lorenzo Bertini, Alberto De Sole, Davide Gabrielli, Giovanni Jona-Lasinio, and Claudio Landim. Macroscopic fluctuation theory. *Rev. Mod. Phys.*, 87(2):593–636, June 2015.
- [33] Gianmaria Falasco, Riccardo Rao, and Massimiliano Esposito. Information Thermodynamics of Turing Patterns. *Phys. Rev. Lett.*, 121(10):108301, September 2018.
- [34] C. Enaud and B. Derrida. Large Deviation Functional of the Weakly Asymmetric Exclusion Process. *J. Stat. Phys.*, 114(3):537–562, February 2004.
- [35] Nahuel Freitas, Jean-Charles Delvenne, and Massimiliano Esposito. Stochastic Thermodynamics of Nonlinear Electronic Circuits: A Realistic Framework for Computing Around kT . *Phys. Rev. X*, 11(3):031064, Sep 2021.
- [36] Nahuel Freitas, Karel Proesmans, and Massimiliano Esposito. Reliability and entropy production in nonequilibrium electronic memories. *Phys. Rev. E*, 105(3):034107, March 2022.
- [37] Massimiliano Esposito. Stochastic thermodynamics under coarse graining. *Physical Review E*, 85(4):041125, 2012.
- [38] Michael Assaf and Baruch Meerson. WKB theory of large deviations in stochastic populations. *J. Phys. A: Math. Theor.*, 50(26):263001, June 2017.
- [39] Rao Riccardo and Leibler Stanislas. Evolutionary dynamics, evolutionary forces, and robustness: A nonequilibrium statistical mechanics perspective. *Proc. Natl. Acad. Sci. U.S.A.*, 119(13):e2112083119, March 2022.
- [40] Shahrezaei Vahid and S. Swain Peter. Analytical distributions for stochastic gene expression. *Proc. Natl. Acad. Sci. U.S.A.*, 105(45):17256–17261, November 2008.
- [41] Pavol Bokes, Alessandro Borri, Pasquale Palumbo, and Abhyudai Singh. Mixture distributions in a stochastic gene expression model with delayed feedback: a WKB approximation approach. *J. Math. Biol.*, 81(1):343–367, July 2020.

Supplementary material for “Emergent second law for non-equilibrium steady states”

Nahuel Freitas¹ and Massimiliano Esposito¹

¹*Complex Systems and Statistical Mechanics, Department of Physics and Materials Science, University of Luxembourg, L-1511 Luxembourg, Luxembourg*

PACS numbers:

I. MODEL FOR THE CMOS MEMORY CELL

We provide here the details of the example given in the main text, based on the model of a non-equilibrium electronic memory developed in [1, 2]. This is a stochastic model of a low-power CMOS memory cell, whose circuit diagram is shown in Figure 1-(a). This circuit involves two identical CMOS inverters, or NOT gates, connected in a loop. Each inverter is in turn composed of a nMOS transistor and a pMOS transistor. The circuit is subjected to a voltage bias $2V_{dd}$, and it has two degrees of freedom: the voltages v_1 and v_2 at the output of each inverter. The total electrostatic energy of the full circuit is $\Phi(v_1, v_2) = (C/2)(v_1^2 + v_2^2) + CV_{dd}^2$, where C is a value of capacitance characterizing the circuit. The internal electronic entropy $S(v_1, v_2)$ is usually neglected in this kind of circuits, and therefore the entropy production is given by the entropy flow alone: $\Sigma = \Sigma_e = -Q/T$, where $-Q$ is the heat dissipated by the circuit.

Each transistor is modelled as a controlled conduction channel (see details in [1]), and two Poisson rates are associated to conduction events in forward and backward directions. In each conduction event, the voltages $v_{1/2}$ can change by the elementary voltage $v_e = q_e/C$. The Poisson rates can be derived from the I-V curve characterization of the transistors and the local detailed balance conditions [1]. For example, for the pMOS transistor in the first inverter one obtains the following Poisson rates (in subthreshold operation):

$$\begin{aligned} \lambda_+^p(v_1, v_2) &= (I_0/q_e) e^{(V_{dd}-v_2-V_{th})/(nV_T)} \\ \lambda_-^p(v_1, v_2) &= \lambda_+^p(v_1, v_2) e^{-(V_{dd}-v_1)/V_T} e^{-(v_e/2)/V_T}, \end{aligned} \quad (1)$$

In the previous equations, $V_T = k_b T/q_e$ is the thermal voltage and I_0 , V_{th} , and n are parameters characterizing the transistor (respectively known as *specific current*, *threshold voltage*, and *slope factor*). Assuming those parameters are the same for all the transistors, the Poisson rates associated to the nMOS transistor in the first inverter are just $\lambda_{\pm}^n(v_1, v_2) = \lambda_{\pm}^p(-v_1, -v_2)$, while the Poisson rates associated to the transistors in the second inverter are given by

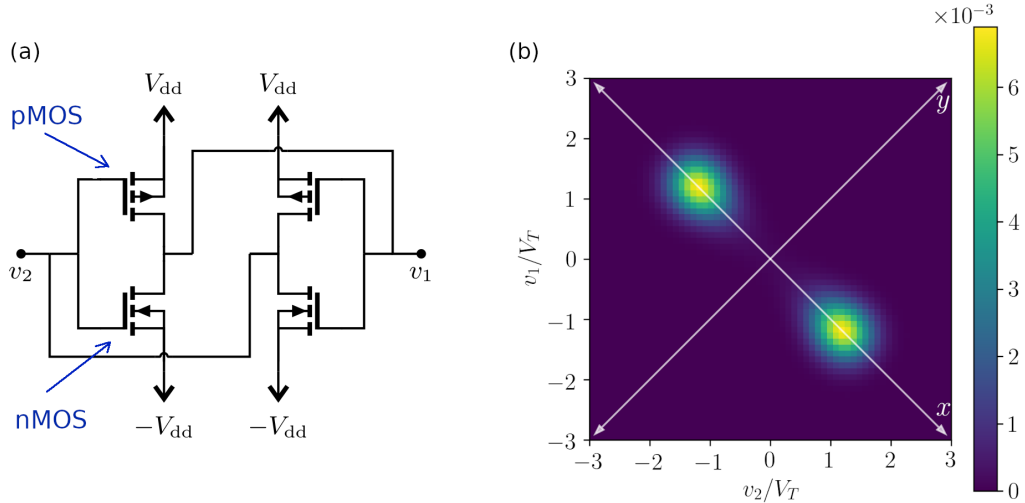


FIG. 1: (a) CMOS implementation of a bistable logical circuit involving two NOT gates in a loop, where each NOT gate is constructed with one pMOS (top) and one nMOS (bottom) transistor. This is the usual way SRAM memory cells are implemented. (b) 2D histogram of the steady state distribution ($v_e/V_T = 0.1$, $V_{dd}/V_T = 1.3$).

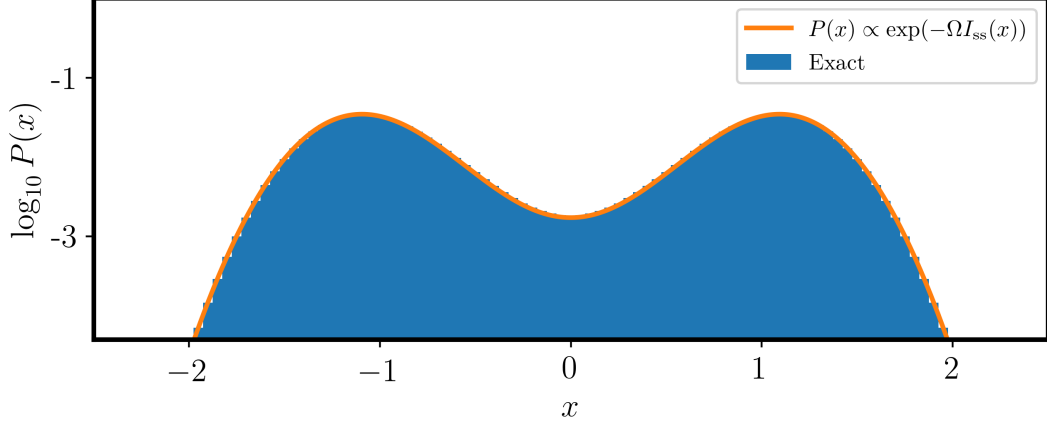


FIG. 2: Comparison between the exact steady state distribution for x and the LD approximation obtained from the rate function $I_{ss}(x)$ in the main text. ($\Omega = 10$ and $V_{dd} = 1.2V_T$).

$\mu_{\pm}^{n/p}(v_1, v_2) = \lambda_{\pm}^{n/p}(v_2, v_1)$. The total rate for a transition $v_1 \rightarrow v_1 + v_e$ is $\tilde{\lambda}_+(v_1, v_2) = \lambda_+^p(v_1, v_2) + \lambda_+^n(v_1, v_2)$, and the total rate for a transition $v_1 \rightarrow v_1 - v_e$ is $\tilde{\lambda}_-(v_1, v_2) = \lambda_-^p(v_1, v_2) + \lambda_-^n(v_1, v_2)$. Then, the state of the system is described by a probability distribution $P(v_1, v_2, t)$ that evolves according to the master equation

$$d_t P(v_1, v_2, t) = P\tilde{\lambda}_+|_{v_1-v_e, v_2} + P\tilde{\lambda}_-|_{v_1+v_e, v_2} + P\tilde{\lambda}_+^*|_{v_1, v_2-v_e} + P\tilde{\lambda}_-^*|_{v_1, v_2+v_e} - P(\tilde{\lambda}_+ + \tilde{\lambda}_- + \tilde{\lambda}_+^* + \tilde{\lambda}_-^*)|_{v_1, v_2}, \quad (2)$$

where we are using the compact notation $PA|_{v_1, v_2} = P(v_1, v_2, t)\tilde{\lambda}_{\pm}(v_1, v_2)$, and $\tilde{\lambda}_{\pm}^*(v_1, v_2) = \tilde{\lambda}_{\pm}(v_2, v_1)$. One can numerically compute the steady state distribution from the previous master equation by truncating the state space to a finite number of states and computing the eigenvector of zero eigenvalue of the master equation generator, or alternatively by Gillespie simulations of the stochastic dynamics. An example is shown in Figure 1-(b), obtained with the former method.

A. Macroscopic limit

A macroscopic limit can be introduced by considering a particular scaling of the physical dimensions of the transistors. In a MOS transistor there are two characteristic dimensions defined with respect to the conduction channel [3]: the length L and the width W . For fixed L , both the capacitance C and the characteristic current I_0 increase linearly with W . Thus, we can consider $\Omega = V_T/v_e \propto W$ as the adimensional scale parameter in the main text. In the following we consider the adimensional voltages v_1 and v_2 , in units of V_T . We also define the scaled rates $\tilde{\omega}_{\pm}(v_1, v_2) = \lim_{\Omega \rightarrow +\infty} \tilde{\lambda}_{\pm}(v_1, v_2)/\Omega$. Then, introducing the large deviations ansatz $P_{ss}(v_1, v_2) \propto \exp(-\Omega I_{ss}(v_1, v_2))$ in the master equation and keeping only the dominant terms in Ω , we obtain the following differential equation for $I_{ss}(v_1, v_2)$:

$$0 = (e^{\partial_{v_1} I_{ss}} - 1) \tilde{\omega}_+(v_1, v_2) + (e^{-\partial_{v_1} I_{ss}} - 1) \tilde{\omega}_-(v_1, v_2) + (e^{\partial_{v_2} I_{ss}} - 1) \tilde{\omega}_+(v_2, v_1) + (e^{-\partial_{v_2} I_{ss}} - 1) \tilde{\omega}_-(v_2, v_1). \quad (3)$$

As shown in [2], evaluating the previous equation at $y \equiv v_1 + v_2 = 0$ leads to a differential equation for the reduced rate function $I_{ss}(x)$ associated to the variable $x \equiv v_1 - v_2$ (this is justified by the contraction principle and the fact that the most probable value of y for any value of x is $y = 0$, see Figure 1-(b)). In that way it is possible to derive the expression for $I_{ss}(x)$ given in the main text. In Figure 2, we compare the probability distribution corresponding to that analytical rate function with exact numerical results. The agreement is essentially perfect even if only a few tens of electrons are involved (the scaling parameter is $\Omega = 10$, and $V_{dd} = 1.2V_T$).

B. Deterministic dynamics

The deterministic equations of motion for the circuit in Figure 1-(a) read:

$$\begin{aligned} CV_T d_t v_1 &= \tilde{\lambda}_+(v_1, v_2) - \tilde{\lambda}_-(v_1, v_2) = i(v_1, v_2) - i(-v_1, -v_2) \\ CV_T d_t v_2 &= \tilde{\lambda}_+(v_2, v_1) - \tilde{\lambda}_-(v_2, v_1) = i(v_2, v_1) - i(-v_2, -v_1), \end{aligned} \quad (4)$$

where $i(v_1, v_2) = I_0 e^{(V_{dd}/V_T - V_{th}/V_T - v_2)/n} (1 - e^{-(V_{dd}/V_T - v_1)})$ is the deterministic electric current through the pMOS transistor for given v_1 and v_2 . Alternatively, in terms of variables x and y defined above,

$$\begin{aligned} CV_T d_t x &= i(x, y) - i(-x, -y) - i(-x, y) + i(x, -y) \\ CV_T d_t y &= i(x, y) - i(-x, -y) + i(-x, y) - i(x, -y), \end{aligned} \quad (5)$$

where the change of variables in the function $i(., .)$ is implicit. Noting that $d_t y|_{y=0} = 0$ for all x , we realize that $y(t) = 0$ for all t if we have $y(0) = 0$. Finally, we note that the total deterministic work rate for given values of votages v_1 and v_2 is $\dot{W} = V_{dd}[i(v_1, v_2) + i(-v_1, -v_2) + i(v_2, v_1) + i(-v_2, -v_1)]$. The scaled work rate defined in the main text is in this case $\dot{w} = \dot{W} v_e / V_T$. The detailed balance drift $\mathbf{u}^{(0)}$ and the lowest order work rate $\dot{w}^{(0)}$ are obtained from the previous expressions by evaluating the currents $i(v_1, v_2)$ at $V_{dd} = 0$. Note also that the deterministic dynamics has a natural timescale $\tau = CV_T / (I_0 e^{-V_{th}/nV_T})$.

C. Vorticity

For this model, the curl or vorticity defined in the last section of the main text reads:

$$\begin{aligned} f(v_1, v_2) &= d_{v_2} \log(\tilde{\omega}_+(v_1, v_2)/\tilde{\omega}_-(v_1, v_2)) - d_{v_1} \log(\tilde{\omega}_+(v_2, v_1)/\tilde{\omega}_-(v_2, v_1)) \\ &\propto \frac{1}{2} \sinh(V_{dd}) (\cosh(v_1 - 2v_2) - \cosh(2v_1 - v_2)) \times \\ &\quad \operatorname{sech}\left(\frac{v_1 - V_{dd}}{2} - v_2\right) \operatorname{sech}\left(v_1 - \frac{v_2 + V_{dd}}{2}\right) \operatorname{sech}\left(\frac{v_1 + V_{dd}}{2} - v_2\right) \operatorname{sech}\left(v_1 - \frac{v_2 - V_{dd}}{2}\right) \end{aligned} \quad (6)$$

II. PROPERTIES OF THE COARSE-GRAINED ENTROPY PRODUCTION

We consider the coarse-grained jump rates $\tilde{\lambda}(\mathbf{n})$ defined in the main text and their macroscopic limit $\tilde{\omega}(\mathbf{x}) = \lim_{\Omega \rightarrow \infty} \tilde{\lambda}(\Omega \mathbf{x}) / \Omega$. The deterministic drift is expressed in terms of these rates as

$$\mathbf{u}(\mathbf{x}) = \sum_{\rho} \tilde{\omega}_{\rho}(\mathbf{x}) \tilde{\Delta}_{\rho} = \sum_{\rho > 0} (\tilde{\omega}_{\rho}(\mathbf{x}) - \tilde{\omega}_{-\rho}(\mathbf{x})) \tilde{\Delta}_{\rho}, \quad (7)$$

and the macroscopic coarse-grained entropy production rate reads:

$$\dot{\pi}(\mathbf{x}_t) \equiv \lim_{\Omega \rightarrow \infty} \dot{\Pi} / \Omega = \sum_{\rho > 0} (\tilde{\omega}_{\rho}(\mathbf{x}_t) - \tilde{\omega}_{-\rho}(\mathbf{x}_t)) \log(\tilde{\omega}_{\rho}(\mathbf{x}_t) / \tilde{\omega}_{-\rho}(\mathbf{x}_t)) \quad (8)$$

If the deterministic dynamics emerging in the macroscopic limit has fixed-point attractors, then $\mathbf{u}(\mathbf{x}^*) = 0$ at the fixed points \mathbf{x}^* . Whenever the set $\{\tilde{\Delta}_{\rho}\}$ of distinct jump vectors is linearly independent, $\mathbf{u}(\mathbf{x}^*) = 0$ implies that $\tilde{\gamma}_{\rho}(\mathbf{x}^*) \equiv \tilde{\omega}_{\rho}(\mathbf{x}^*) - \tilde{\omega}_{-\rho}(\mathbf{x}^*) = 0$ for all ρ . As a consequence, the entropy production rate in Eq. (8) vanishes at the fixed points. The linear independence assumption is always satisfied for electronic circuits. It might fail to hold for some chemical reaction networks, but it can be restored by adding intermediate steps in some reactions (effectively increasing the dimensionality of the system).

The fact that the macroscopic coarse-grained entropy production vanishes at the fixed points of the deterministic dynamics does not imply that the model is detailed-balanced at the coarse-grained level. The model will be effectively detailed-balanced if and only if the log-ratio $\tilde{\sigma}_{\rho}(\mathbf{x}) \equiv \log(\tilde{\omega}_{\rho}(\mathbf{x}) / \tilde{\omega}_{-\rho}(\mathbf{x}))$ can be derived from a gradient, i.e., if $\tilde{\sigma}_{\rho}(\mathbf{x}) = -\tilde{\Delta}_{\rho} \cdot \nabla \tilde{\phi}(\mathbf{x})$ for some function $\tilde{\phi}(\mathbf{x})$. Whenever the set $\{\tilde{\Delta}_{\rho}\}$ is also orthonormal (as it is for the example in the previous section), one can check if $\tilde{\sigma}_{\rho}(\mathbf{x})$ derives from a gradient by checking if the generalized curl $f_{\rho, \rho'}(\mathbf{x}) \equiv \partial_{x_{\rho}} \tilde{\sigma}_{\rho'}(\mathbf{x}) - \partial_{x_{\rho'}} \tilde{\sigma}_{\rho}(\mathbf{x})$ vanishes for all ρ, ρ' , and \mathbf{x} .

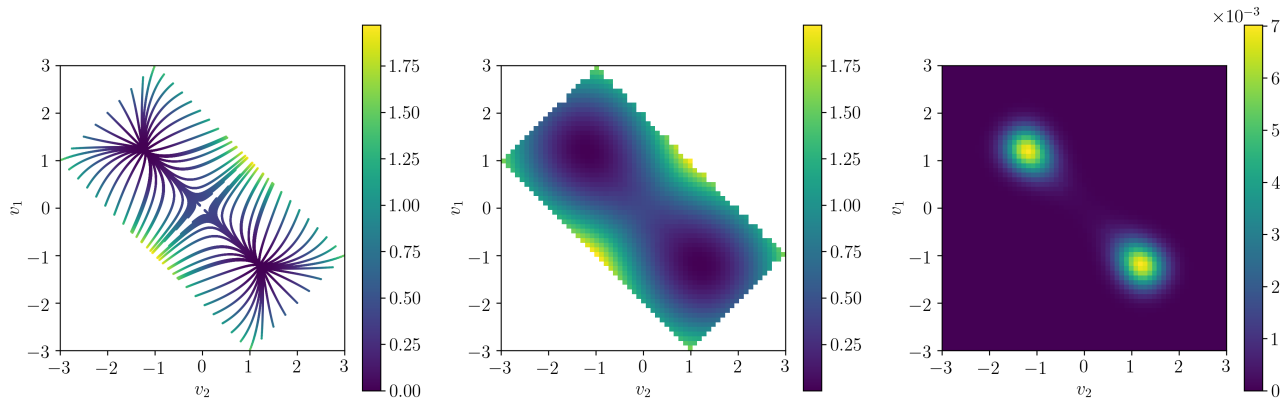


FIG. 3: (a) A set of deterministic trajectories converging to the fixed points. The color of each point indicates the value $\pi = \int_0^{+\infty} dt' \dot{\pi}(\mathbf{v}_{t'})$ of the scaled coarse-grained entropy produced during the relaxation from that point until the fixed point, which according to the emergent second law is an upper bound to the true steady state rate function. (b) 2D linear interpolation of the data in (a). (c) Probability distribution obtained as $P_{\text{rec}} \propto e^{-I_{\text{rec}}/v_e}$, where I_{rec} is the estimation of the rate function in (b). The parameters are the same than in Figure 1-(b).

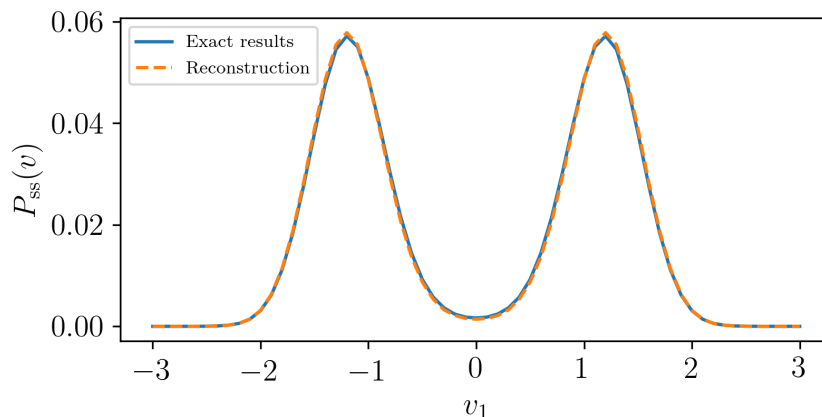


FIG. 4: Comparison of the partial distribution for the variable v_1 as obtained from the exact steady state of Figure 1-(b) and the reconstructed one in Figure 3-(c).

III. FULL RECONSTRUCTION OF THE STEADY STATE DISTRIBUTION

In this section we illustrate how the emergent second law can be employed as an alternative to stochastic simulations (for example the Gillespie algorithm) or spectral methods (finding an eigenvector of the master equation generator) in order to compute non-equilibrium steady state distributions. The strategy is to cover the state space with a sufficiently dense set of deterministic trajectories. Then, a bound for the steady state rate function can be obtained along each of the trajectories. If this bound is obtained from the coarse-grained entropy production, instead of the physical one, we know that at least close to deterministic fixed points the bound will be tight (since by construction the coarse-grained currents vanish at the fixed points, and the bound is tight close to equilibrium). In the particular case of the CMOS memory, we know that the bound is also an accurate approximation of the rate function far away from the fixed point. This procedure is shown in Figure 3. In Figure 3-(a) we show a set of deterministic trajectories, each of which is colored in a way that indicates the value of the bound to the rate function as given by the emergent second law, and that in the following will be considered an estimation of the actual rate function. In Figure 3-(b) we interpolate the data in Figure 3-(a) using the ‘griddata’ function of the SciPy suite [4] with the ‘linear’ interpolation method. The rate function reconstructed in this way is employed to produce the probability distribution shown in

Figure 3-(c). The parameters employed are the same than for the exact distribution in Figure 1-(b), and the fidelity between the exact and the reconstructed distribution is very high. As an example, we show in Figure 4 the partial distribution for v_1 according to both results.

